JMEPEG (2004) 13:564-574
DOI: 10.1361/15477020420819

1059-9495/$19.00

Fatigue Life Improvements of the AISI 304 Stainless Steel Ground Surfaces by Wire Brushing

Nabil Ben Fredj, Mohamed Ben Nasr, Amir Ben Rhouma, Chedly Braham, and Habib Sidhom

(Submitted December 21, 2003)

The surface and subsurface integrity of metallic ground components is usually characterized by an induced tensile residual stress, which has a detrimental effect on the fatigue life of these components. In particular, it tends to accelerate the initiation and growth of the fatigue cracks. In this investigation, to deliberately generate compressive residual stresses into the ground surfaces of the AISI 304 stainless steel (SS), wire brushing was applied. It was found that under the experimental conditions selected in this investigation, while the surface roughness was slightly improved by the brushing process, the surface residual stress shifted from a tensile stress ($\sigma_{\parallel}$ = +450 MPa) to a compressive stress ($\sigma_{\parallel}$ = −435 MPa). On the other hand, the work-hardened deformation layer was almost two times deeper after wire brushing. Concerning the fatigue life, an improvement of 26% in terms of endurance limit at 2×10^6 cycles was realized. Scanning electron microscope (SEM) observations of the fatigue fracture location and size were carried out to explain the fatigue life improvement. It was found that the enhancement of the fatigue strength could be correlated with the distribution and location of the fatigue fracture nucleation sites. Concerning the ground surfaces, it was seen that the fatigue cracks initiated at the bottom of the grinding grooves and were particularly long (150-200 μm). However, the fatigue cracks at the brushed surfaces were shorter (20-40 μm) and appeared to initiate sideways to the plowed material caused by the wire brushing. The results of the wire-brushed surface characterization have shown that significant advantages can be realized regarding surface integrity by the application of this low-cost process compared to shot peening.

Keywords fatigue life, grinding, residual stress, wire brushing

1. Introduction

The material removal mechanism for the grinding process can be characterized by the formation of microchips generated by the cutting edges of the abrasive grits. This specific mechanism for material removal in a machining process offers wide applications to surfaces requiring high geometrical quality with tightened tolerances even for materials usually classified as difficult to cut (i.e., ceramics).[1] However, as chip formation occurs by intense shearing, in an extremely thin zone, under very high deformation rates, and at very short times, the heat that is generated by the plastic flow and friction can be conducted away from the grinding zone. This leads to surfaces with low integrity having problems such as surface burning, material redeposition, surface and subsurface cracking, mechanical and metallurgical transformations of the upper layers of the workpiece,[2,3] and surface tensile residual stresses. These characteristics and, in particular, the magnitude of the tensile surface residual stress were found to affect significantly the fatigue lives of mechanical components[4-6] that have undergone grinding by accelerating the initiation and the propagation of the fatigue cracks. On the other hand, it was found that the near-surface compressive residual stresses usually extend the fatigue life.[7,8] To consider these findings with respect to in-service applications of ground components, compressive residual stresses have to be introduced to their surfaces. This can be done by selecting fine grinding conditions with low work speeds and small cut depths, and, if necessary, the use of costly grinding wheels with special abrasive grits like SG, CBN, or diamond.[9] These solutions were found to affect substantially the cost of the grinding operation, as they lower the process productivity and induce additional expenses for the acquisition and preparation of the grinding wheels.[10]

Another way of deliberately compressing the surface and near-surface layers of the ground components consists of using additional surface treatments such as polishing, shot peening,[11-15] deep rolling,[16] laser shock peening,[17,18] ball burnishing,[19] ultrasonic impact treatment,[20] surface coating,[21] and/or surface nitriding.[22] Some results of published data, related to the improvement rates of the fatigue strength resulting from these treatments, are reported in Table 1. This table shows that the improvement in fatigue strength ranged from 9-36%, depending on the treatment type, treatment conditions, treated materials, and machining process. Table 1 also shows that laser shot peening and shot peening significantly affect the surface roughness of the initial state generated by the previous machining operation. This fact has to be taken into account when such surface treatments are considered for surfaces requiring low roughness. The other main parameters that have to be considered when selecting the surface treatment process are the cost of the treatment and the geometry of the treated components. Indeed, while the industrial applications of ball burnishing and deep rolling are usually limited to rotationally symmetric components (e.g., shafts), hammer and shot peening

Nabil Ben Fredj, Mohamed Ben Nasr, Amir Ben Rhouma, and **Habib Sidhom,** Laboratoire de Mécanique, Matériaux et Procédés, LAB-STI-03, ESSTT, 5, Avenue Taha Hussein, 1008, Tunis, Tunisia; and **Chedly Braham,** Laboratoire de Microstructure et Mécanique des Matériaux, ENSAM, CNRS ESA 8006, 75013 Paris, France. Contact e-mail: nabil.benfredj@esstt.rnu.tn.

Table 1 Improvements of machined surface integrity resulting from different posttreatment operations

Material	Machining conditions	Surface characterization			Fatigue resistance			
		Hardening(a)	Residual stress, MPa	Roughness (R_a), μm	σ_D, MPa	N(b), approx	Specimen	Nucleation sites
AISI 4340	Gentle grinding	…	−350	…	827	2×10^5	Notched	Surface
	…	…	…	…	…	…	Not notched	…
AISI 52100	Grinding	…	−40	…	…	…	Notched	Surface
AISI 5140	Grinding	…	−30	…	…	…	Notched	Surface
AISI 5120	Grinding	…	−50	…	…	…	Notched	Surface
AISI Al12SI-T6	Milling	…	…	…	103	…	Notched	Surface
AISI A356-T6	Milling	…	…	0.7	110	…	Notched	Surface
AISI 7075-T6	Milling	…	…	0.6	190	…	Notched	Surface

Material	Posttreatment conditions	Surface characterization			Fatigue resistance				Fatigue improvements, %	Reference
		Hardening (a)	Residual stress, MPa	Roughness (R_a), μm	σ_D, MPa	N(b), approx	Specimen	Nucleation sites		
AISI 4340	Low plasticity burnishing	…	−1100	…	1033	7×10^5	Notched	Subsurface	25	14
AISI 4340	Shot peening									
	0.0027 A	…	−950	…	830	…	Not notched	Subsurface	9	15
	0.0063 A	…	−1100	…	900	…	Not notched	Subsurface	12	15
	0.0083 A	…	−1200	…	865	…	Not notched	Subsurface	10	15
	0.0141 A	…	−1300	…	845	…	Not notched	Subsurface	10	15
AISI 52100	Shot peening	…	−880	…	…	…	Notched	Subsurface	10	16
AISI 5140	Shot peening	…	−750	…	…	…	Notched	Subsurface	15	16
AISI 5120	Shot peening	…	−570	…	…	…	Notched	Subsurface	18	16
AISI Al12SI-T6	Laser shot peening	…	−125	…	126	…	Notched	Subsurface	22	17
AISI A356-T6	Laser shot peening	10	−145	1.1	150	…	Notched	Subsurface	36	17
	Shot peening	20	−210	5.8	…	…	…	…	…	17
AISI 7075-T6	Laser shot peening	10	−300	1.3	236	…	Notched	Subsurface	23	17
	Shot peening	20	−340	5.7	215	…	…	Subsurface	12	17

(a) Hardening $= \Delta H_v / H_v \times 100$. H_v, initial hardness. (b) N, number of cycles in fatigue test

are frequently applied to the external surfaces of mechanical components. Concerning laser shot peening, ultrasonic impact treatment, and surface coating, even though promising results were reported by recent investigations,[17,18,20] they remain costly, and their applications are restricted to components with complicated geometry for which other techniques cannot be used.

Another method that can introduce compressive residual stresses into the upper layers of the surfaces of mechanical components by cold plastic deformation is wire brushing. This low-cost, fast, and easy technique is commonly used for online polishing, deburring, and removing thin contaminated layers. Recently developed brushing methods use robotic systems for automated deburring and applications for finishing of surfaces having complex geometries.[23,24] However, even though it is known that the brush stiffness, rotational speed, and force exerted on the workpiece play crucial roles in establishing the material removal rate and surface finish quality, limited information is available in the literature pertaining to the brushed surface integrity, particularly the improvements in the fatigue life of brushed components. One class of material in which wire brushing has been considered is stainless steel (SS). In fact, the investigation conducted by Ben Rhouma et al.[24] showed substantial improvements in pitting, crevice, and corrosion resistance under stress in an aggressive medium for the brushed surfaces of AISI 316L SS. These improvements were explained by the fact that the brushing process induces additional hardening by plastic deformation, leading to compressive residual stresses in the treated surfaces. Based on these findings, and to continue investigating the improvements of machined surface integrity resulting from the application of the wire-brushing process, experiments were conducted to evaluate the fatigue life enhancements of the AISI 304 SS ground surfaces. The brushing conditions were optimized on the basis of criteria related to induced residual stress, work hardening, surface roughness, and burr formation. In the second step, three-point bending fatigue tests were conducted on ground and brushed specimens to evaluate the endurance limit improvements at 2×10^6 cycles. The mechanisms of fatigue crack initiation and propagation were investigated based on scanning electron microscope (SEM) observations of the fatigue fracture surface of the tested specimens. The role of work hardening and residual stress on fatigue crack nucleation and growth were established.

2. Experimental Procedures

2.1 Materials

The material used in this study was AISI 304 SS, for which the chemical composition and the mechanical properties are given in Tables 2 and 3, respectively. Figure 1 shows a micro-

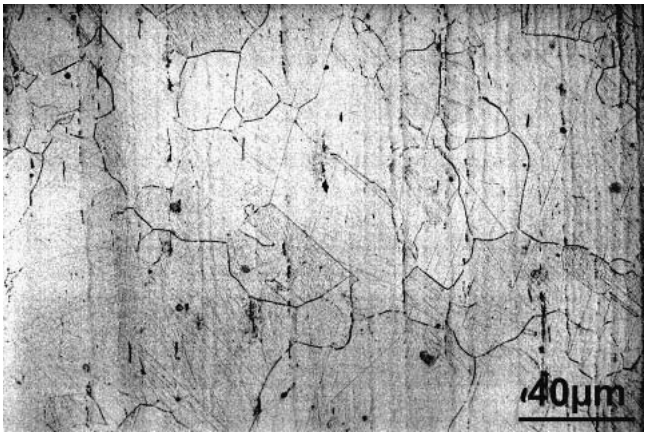

Fig. 1 Austenitic structure of the AISI 304 SS specimen

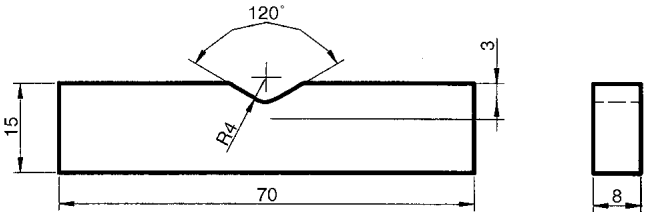

Fig. 2 Geometry of fatigue test specimen (stress concentration factor, $K_t = 1.6$; all dimensions are in millimeters)

Table 2 Chemical composition

C	Si	Mn	Cr	Ni	Mo	Cu	N	Fe
0.05	0.41	1.14	18.04	9	0.193	0.0348	0.004	balance

graph of the AISI 304 SS microstructure. It has an average grain size of 150 μm.

2.2 Surface Preparation

A notched fatigue-flexture specimen with a stress concentration factor of $K_t = 1.6$ was selected (Fig. 2). The main advantage obtained from using this geometry is that localized crack initiation starts at the notch root.

The notch was machined into the sample on an NC milling machine using an endmill having a diameter of 8 mm. Specimens were subsequently subjected to a stress relief annealing treatment (i.e., heating at 1050 °C over the course of 1 h followed by air cooling) before being ground and/or wire-brushed. Only the notch was ground using a V-shaped grinding wheel. The grinding conditions are summarized in Table 4.

The experimental setup used for the wire-brushing experiments is shown in schematic form in Fig. 3. An SS wire brush was used for the experiments. This brush was set on a conventional milling machine. During the wire-brushing process, the wires were effectively compressed by 3% of their length (i.e., the surface of the notch was set at 2.4 mm from the inner end of the wires). The experimental conditions under which the brushing tests were conducted are listed in Table 5.

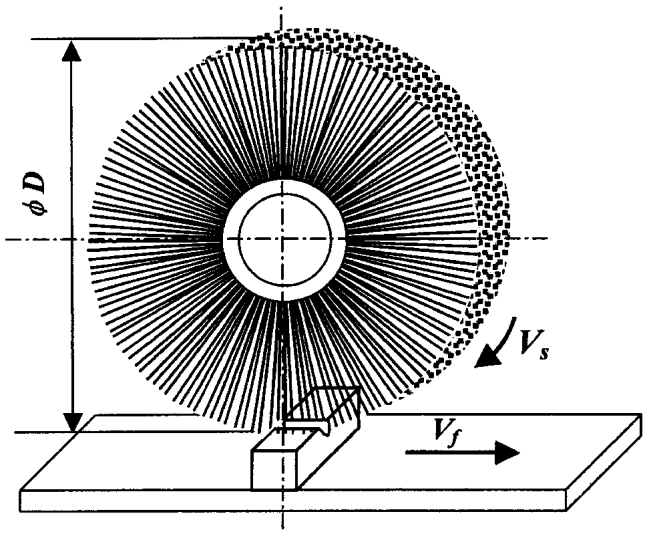

Fig. 3 Schematic view of the wire-brushing experimental setup and parameters

Table 3 Mechanical properties

Yield stress	R_m, MPa	A, %	Microhardness (H_v)	Toughness at 20 °C, J/cm^2
315	690	58	172	270

Table 4 Grinding conditions

Conditions	Set condition
Grinding mode	Plunge surface grinding, down cut
Grinding wheel	99 A 46 M 7 V 10 N with V shape
Stock removal rate	$Z' = 30$ mm^3/mm/min
Wheel speed	$V_s = 30$ m/s
Work speed	$v_w = 5$ m/min
Depth of cut	$a = 6$ μm
Environment	Soluble oil (20%), 7.2 L/min
Workpiece material	AISI 304 SS
Dresser	Single-point diamond dresser
Dressing depth	0.01 mm
Cross feed	0.2 mm/revolution
Environment	Dry

2.3 Testing Methods

The ground and brushed surfaces were characterized by roughness measurements using a stylus-type profilometer. Surface hardening was characterized by microhardness measurements using a microhardness tester set at a load of 50 g_f. The surface residual stresses were evaluated using the x-ray method under the conditions listed in Table 6. Due to the coarse grain size of the AISI 304 SS specimens, it was difficult to measure the depth of residual stresses using this technique. Therefore, residual stress was also evaluated using the hole-drilling method.[24] Holes were drilled incrementally using a 2 mm diameter drill rotating at a high cutting speed (2500 rpm) to avoid inducing additional residual stresses. High-cycle fatigue tests (up to 2×10^6 cycles) were performed using a three-point bend geometry. For all fatigue experiments, the stress ratio was fixed to $R = 0.1$ and the test frequency to 15 Hz.

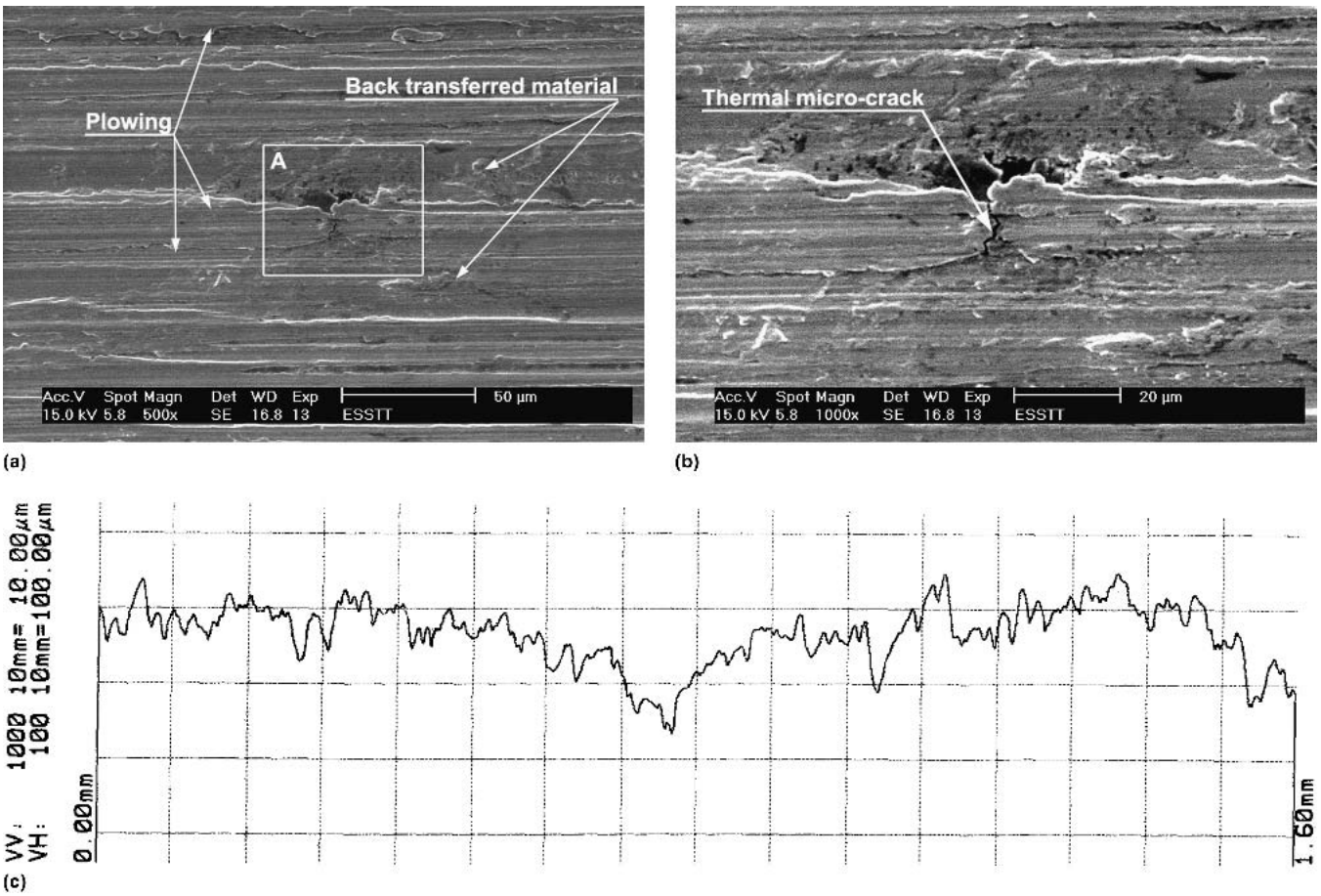

Fig. 4 **(a)** General aspect of the ground surface of the AISI 304 SS specimen. **(b)** Thermal microcracks at the bottom of the grinding groove (detail A in (a). (**c**) Roughness profile of the ground surface (R_a = 2.2 µm; R_t = 16.5 µm)

To better understand the effects of mechanical and thermal loading on the surface quality corresponding to each surface finishing mode, force components and the surface temperature generated by the grinding wheel and the wire brush were measured. Forces were measured using a piezoelectric transducer dynamometer (model 9257B, Kistler, Kirkland, WA). The surface temperature was measured using a thermocouple with a wire diameter of 25 µm.[10]

3. Results

3.1 Optimization of the Wire-Brushing Conditions

Previous investigations have shown that the main surface integrity parameters controlling the fatigue behavior of the mechanical components are the residual stress, the surface roughness, and the induced work hardening.[18-20,25,26] Therefore, wire brush optimization was made on the basis of criteria related to high compressive residual stress, high work hardening, low surface roughness, and small size of burr formation by the brushing process. Indeed, the main industrial application of the wire brushing remains deburring. On the other hand, even though the wire diameter and length are supposed to have significant effects on surface integrity, in this investigation, as the same brush was used for all the experiments, the optimized brushing conditions considered were the brush rotational speed, the work speed, and the number of passes.[24] The effective wire compression was fixed at 3% of the wire length. Table 7 summarizes the experimental conditions considered for optimization and the corresponding results. All brushed specimens were first ground under the conditions listed in Table 4. The surface roughness parameters generated by the grinding process were R_a = 2.2 µm and R_t = 16.5 µm. R_a is the arithmetic average surface roughness and R_t is the maximum surface roughness.

Analyzing the results given in Table 6 leads to the conclusion that two brushing conditions have to be considered as they offer the highest compressive residual stresses. These conditions correspond to sets S_2 and S_4. In terms of productivity, S_4 is more interesting as it takes only 12 s to finish brushing a 1 mm length compared with S_2, which takes 14 s to brush the same length. On the other hand, even though no significant difference in surface roughness is observed between these two conditions, increased work hardening was realized using the S_2 set of conditions. Moreover, it was observed that the height of the induced burr was much lower when brushing under S_4 conditions. These observations suggest the use of S_4 for wire brushing the fatigue test specimens. Concerning the brushing conditions of set S_1 (brush speed, or V_s = 2000 rpm; work speed, V_f = 12.5 mm/min; N = three passes), a substantial

Table 5 Brushing conditions

Conditions	Set condition
Wire material	SS
Brush diameter	D = 230 mm
Wire diameter	ϕ = 0.1 mm
Wire length	l = 80 mm
Brush rotational speed	V_s = 800, 1250, and 2000 rpm
Work speed	V_f = 50 mm/min
Number of passes	N = 3, 5, and 10 passes
Percentage of effective wire compression	3%

Table 6 X-ray diffraction parameters

Parameter	Set parameter				
Radiation	λ Mn K_α x λ = 0.2102 nm				
Voltage	20 kV				
Current	5 mA				
X-ray diffraction planes	{3 1 1} 2θ ≈ 152°				
Beam diameter	2 mm				
ϕ angles	0° and 90 °				
ψ oscillation	±3°				
ψ angles	−3727	−33.21	−28.88	−24.09	−18.43
	−10.52	0.00	14.96	21.42	26.57
	31.09	35.26	39.23		

thermal effect on the brushed surface and on the brush wires was noticed. The surface temperature of the sample increased, and the metallic wires of the brush were damaged. Indeed, under these conditions, a burr was formed by the welded microfragments of the brush wires.

3.2 Ground and Brushed Surfaces Integrity

Table 8 gives the values of the parameters, which were selected to characterize the surface integrity and the fatigue behavior of the AISI 304 SS in the ground and brushed states. Table 8 also gives the force components and temperature values generated during the process. These parameters were selected as they help in understanding the fatigue behavior of the tested specimens.

3.3 Surface Microgeometrical Quality

3.3.1 Ground Components. SEM observations of the ground surfaces, which are shown in Fig. 4(a), highlight the back transfer of workpiece material. Sideways displacement of the workpiece material from grinding, through a plowing mechanism, is also observed. Moreover, microcracks with a length of 20 μm, which likely were generated by thermal effects, are seen at the bottom of the grinding grooves (Fig. 4b). On the other hand, the ground surface roughness profile topography (Fig. 4c) exhibits irregularly spaced, nonuniform sharp peaks and valleys. This surface morphology is expected to affect significantly the fatigue crack initiation of the AISI 304 SS ground specimens.

3.3.2 Brushed Components. Brushed specimens (Fig. 5a) show similar morphology to the shot-peened surfaces. Plowing by plastic deformation results from the successive passes of the wire brush. The grinding grooves are completely eliminated by the brushing process, and no trace of these grooves can be seen even at high magnification (Fig. 5b). The brushed surface roughness profile, which is shown in Fig. 5(c), shows a topography having fewer high irregularities with less sharpness than the roughness profiles of the ground surfaces. This explains the reduction of the R_t observed in column D of Table 8.

3.4 Work Hardening

Profiles of Vickers microhardness ($H_{v0.05}$) for the ground and wire-brushed surfaces are shown in Fig. 6. Figure 6 shows that wire brushing leads to higher work hardening at the surface and is equivalent in depth to that obtained by grinding. Indeed, the work-hardening rate generated by the brushing process is almost twice as high as that induced by the grinding process (Table 8, column C).

3.5 Residual Stress

3.5.1 Ground Components. The distribution of residual stresses induced by the grinding process is illustrated by the profiles in Fig. 7(a). The main characteristics of these profiles are summarized in Table 8 (column E), which shows that the upper ground layers are particularly subject to tensile residual stresses in both directions. The higher levels of these stresses are achieved at a depth of 50-100 μm, with $\sigma_{\parallel max}$ = +600 MPa and $\sigma_{\perp max}$ = +530 MPa. The lower levels of these stresses were measured on the ground surfaces using the x-ray technique ($\sigma_\parallel$ = +450 MPa; $\sigma_\perp$ = +350 MPa) and are probably due to the relaxation effects of these stresses resulting from the microcracks generated by the thermal loading of these surfaces (Fig. 4b).

3.5.2 Brushed Components. The residual stress profiles in Fig. 7(b) show the stress distribution measured for the wire-brushed surfaces. It should be noted that the residual stresses shift to compressive ones and that the highest levels of the residual stresses are reached at a depth of 30-50 μm. However, less difference between the surface values ($\sigma_\parallel$ = −435 MPa; $\sigma_\perp$ = −220 MPa) and the maximum values ($\sigma_\parallel$ = −514 MPa; $\sigma_\perp$ = −233 MPa) of the residual stresses are observed in this case.

3.6 Fatigue Behavior of the Ground and Brushed Specimens

The stress, number of cycles (*S-N*) curves of Fig. 8 show the fatigue life of the ground and wire-brushed specimens subjected to constant amplitude loading. Fatigue tests were stopped beyond 2×10^6 cycles if no fracture occurred. Clearly, the fatigue life of the brushed specimens was significantly higher than that of the ground specimens. For $N > 10^6$ cycles, the fatigue strength, as characterized by the endurance limit σ_D, increased by 26% for the ground and brushed specimens (Table 8, column H). For an applied loading corresponding to σ_{max} = 280 MPa, Fig. 8 shows that the fatigue life of ground specimens can be multiplied by a factor of 10 when wire brushing is applied to these surfaces.

3.7 Fatigue Crack Nucleation and First-Stage Propagation

Different fatigue crack nucleation mechanisms could be observed depending on the surface preparation mode. These ob-

Table 7 Wire-brushing tests conditions and surface layers characterization results

Set number	Brushing conditions: Brush speed (V_s), rpm	Brushing conditions: Work speed (V_f), mm/min	Brushing conditions: No. of passes, N	Residual stress, MPa: $\sigma\|\|$(a)	Residual stress, MPa: $\sigma\perp$(b)	Cold work-hardening rate: $\Delta H_v/H_v$, %	Surface roughness, μm: R_a	Surface roughness, μm: R_t	Average height of induced burr, mm
S_1	2000	12.5	3	−245 ± 50	−85 ± 50	94	2.45	13.35	0.83
S_2	1250	12.5	3	−415 ± 40	−385 ± 50	78	2.12	11.64	0.42
S_3	800	12.5	3	−245 ± 40	−300 ± 40	66	2.35	15.24	0.2
S_4	800	50	10	−435 ± 20	−220 ± 35	140	2.21	10.22	0.15

(a) Stress measured in the same direction as V_f (Fig. 3, Table 6). (b) Stress measured in a perpendicular direction to V_f (Fig. 3, Table 6)

Table 8 Effects of surface preparation mode on surface quality

	Surface characteristics: A		B	C	D		E	
	Process force components, N/mm		Surface temperature, (θ), °C	Cold work-hardening rate ($\Delta H_v/H_v$), %	Surface roughness, μm		Residual stress, MPa	
Surface preparation	F'_n	F'_t			R_a	R_t	$\sigma_\|$(a)	$\sigma\perp$(b)
Grinding	2.2	1.4	542	82	2.2	16.5	+450 ± 15	+350 ± 20
Brushing after grinding	1.5	0.8	85	140	2.2	10.2	−435 ± 20	−220 ± 35

	Surface characteristics: F	G	H		I	
			Endurance limit $\sigma_D = \sigma_{max}$, MPa 2×10^6 cycles		S–N graph parameters $N \times \sigma^m = C$	
Surface preparation	Surface damage	Phase change	σ_D	Improvement (c), %	C	m
Grinding	Trace of surface burning	No change	226 ± 10	…	2951×10^{18}(d)	5.82(d)
Brushing after grinding	No trace of burning	No change	285 ± 10	26	7316×10^{25}(e)	9.47(e)

(a) Stress was measured in the same direction as V_f (Fig. 3, Table 5). (b) Stress measured in a perpendicular direction to V_f (Fig. 3, Table 5). (c) The percentage of improvement is defined as $[(\sigma_{DB} - \sigma_{DG})/\sigma_{DG}] \times 100$ where σ_{DG} is the endurance limit of the ground specimens and σ_{DB} is the endurance limit of the brushed one. (d) $R^2 = 0.9745$. (e) $R^2 = 0.9536$

servations were made through SEM microfractographic analysis of the fracture surfaces of the fatigue-tested specimens.

3.7.1 Ground Surface. SEM observations of the fatigue-tested specimens near the fracture surface (Fig. 9a) show that the fatigue cracks of the ground specimens are particularly long with an average length of 150-200 μm. It is also seen that crack nucleation takes place at the surface and likely initiates at the bottom of the grinding grooves, which had previously been reported as sites of thermal microcracks. On the other hand, observations of the associated fracture facets (Fig. 9b) show a brittle crystallographic first-stage propagation mode.

3.7.2 Brushed Surface. The lengths of the fatigue cracks observed on the brushed surfaces of the fatigue-tested specimens (Fig. 10a) are shorter than those seen on the surfaces of the ground samples that had been subjected to the same fatigue experiments. In this case, the average crack length was on the order of 20-40 μm. Figure 10(a) also shows that these small cracks are particularly concentrated around the displaced material that had been formed by plowing and that result from the successive passes of the wire brush.

3.8 Fatigue Crack Propagation

The mechanism of fatigue crack propagation far from the affected layers by the applied surface preparation mode seems to be similar. This mechanism is particularly characterized by the formation of fatigue striation resulting from ductile fracture mode at these depths (Fig. 9c). At the overload zone, corresponding to final fracture, dimples resulting from the well-known ductile fracture of the AISI 304 SS were observed (Fig. 9d).

4. Discussion

4.1 Surface Quality Improvements Resulting From the Application Brushing Process

Results from this investigation have shown that substantial improvements of the ground surface quality of the AISI 304 SS can be realized by the application of the wire-brushing process. It was observed that this process results in superficial material removal, which is just enough to reduce or completely erase the sideways flow by plowing, burrs, microcracks, and the near-

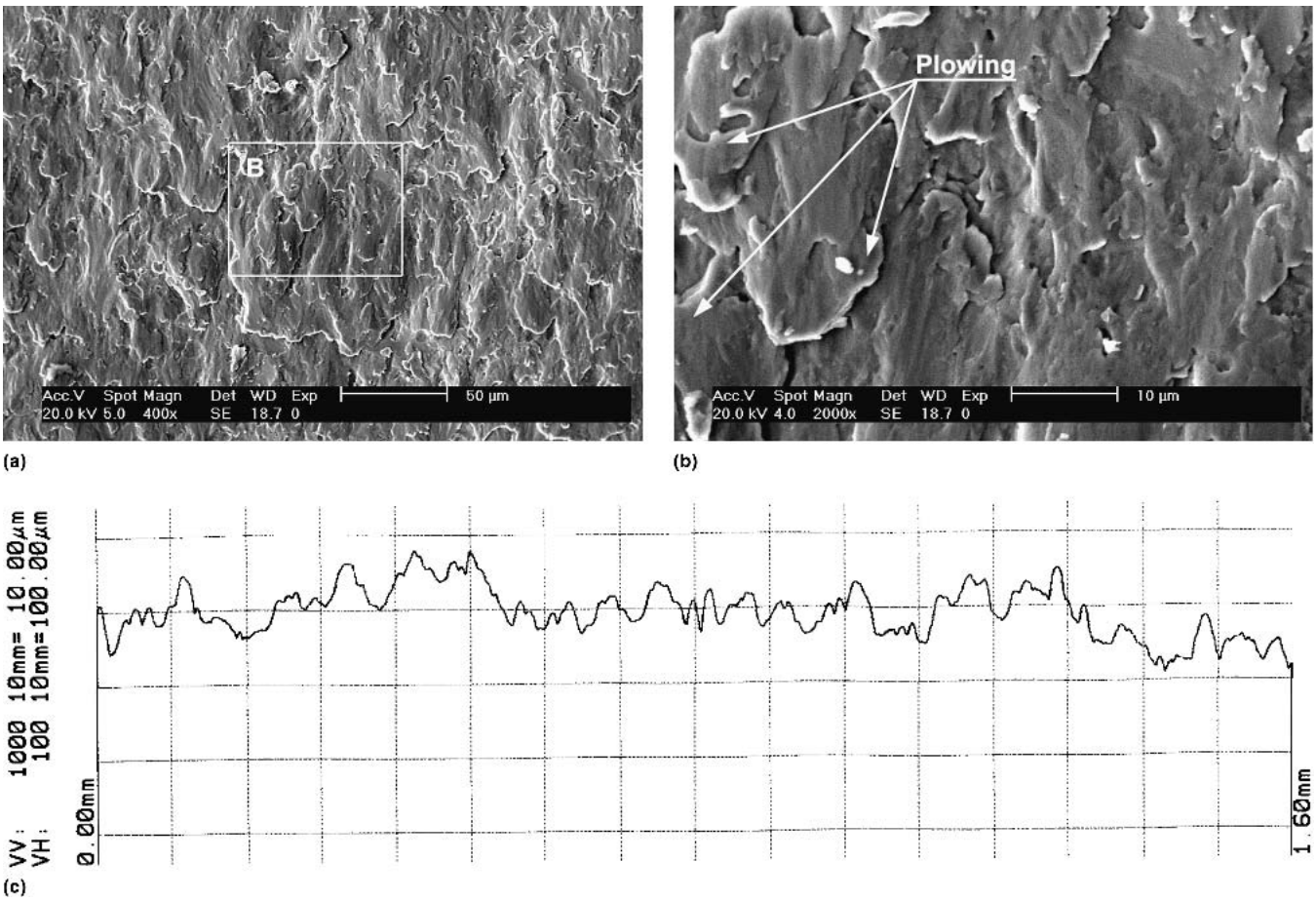

Fig. 5 (**a**) General aspect of the wire-brushed surface of the AISI 304 SS specimen. (**b**) Plowing by plastic deformation of the brushed surface (detail B in (a). (**c**) Roughness profile of the wire-brushed surface (R_a = 2.2 μm; R_t = 10.2 μm)

surface tensile residual stress distribution generated by the grinding process. The ground surface quality improvements realized by the application of the brushing process can be summarized as follow:

- Improvement of the surface microgeometrical quality, which is characterized by a lower value of the parameter R_t resulting from the plastic deformation of the ground surface generated by the successive passes of the wire brush. Within the experimental conditions used in this investigation, R_t could be reduced to about 60% of the initial value. Moreover, no traces of surface burning or microcracks were observed. On the other hand, roughness profiles have shown that while the ground surface is characterized by a sharp topography, a smoother one was observed for the brushed surface. When these results were compared with those obtained using a shot-peening process,[27] it could be concluded that the wire-brushing process provides surfaces with almost the same level of compressive residual stress and work hardening. However, wire-brushed surfaces present higher microgeometrical quality compared with the shot-peened ones. Indeed, it was reported that when surfaces of the AISI 304 SS were shot peened using steel shot with a diameter of 1.2 mm, and at a rate of 1.2 s/cm^2, a compressive residual stress with maximum amplitude of −650 MPa and maximum work hardening of $H_{v0.05}$ = 430 could be generated. However, under these shot-peening conditions, the surface roughness parameters were R_t = 41.1 μm and R_a = 4.7 μm. These values are high compared with those obtained using the brushing process (R_t = 10.2 μm; R_a = 2.1 μm). This difference is related to the fact that shot peening induces, depending upon the shot intensity, overlaps, scaling, and microcracks resulting from excessive material deformation, and is responsible for the low surface microgeometrical quality. By considering the detrimental effects of the surface roughness on fatigue lifetime, it is expected that at equivalent levels of compressive residual stress and work hardening, the wire-brushed specimens would give higher fatigue resistance than the shot-peened ones.
- Improvement of the quality of the surface, and the near surface layer by work hardening, results in higher surface hardness and thicker hardened layer with no trace of surface microfracture. Improvement of the residual stress distributions, which shifts from tensile for the ground surfaces to compressive for the wire-brushed ones, is independent of the measuring direction. Concerning the ground surface, it was found that the maximum tensile

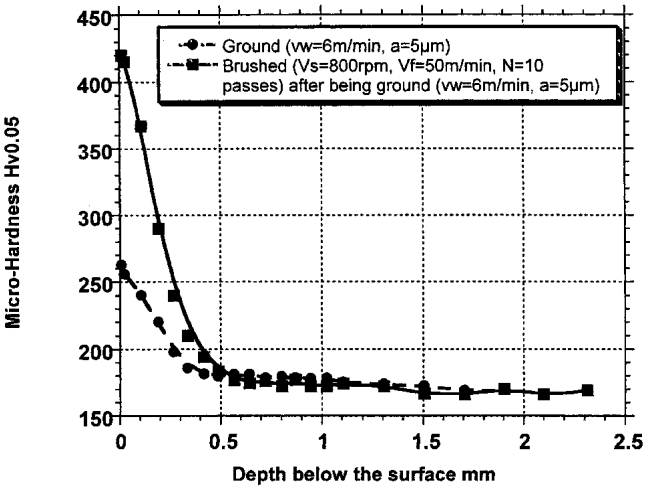

Fig. 6 Work hardening of the AISI 304 SS specimen induced by the grinding and brushing processes

residual stress was in the subsurface region. The lower value of residual stress, measured at the ground surface, may be explained by the relaxation effects of these stresses resulting from surface microcracks generated by the high thermal loading of these surfaces. Indeed, according to Table 8, column A, the specific grinding energy, which is the energy per unit volume of material removal, can be calculated using the following formula[1]:

$$U = \frac{F'_t V_s}{v_w a}$$

where F'_t is the specific tangential grinding force, V_s is the grinding wheel peripheral speed, v_w is the work speed, and a is the grinding depth of the cut. Using the experimental values from Table 4, an energy density of 132 J/mm^3 is needed to remove 1 mm^3 AISI 304 SS. This value is significantly higher than the value reported in Ref 28 where it was indicated that even with U = 70 J/mm^3, microcracks and microvoids characterize the ground surface morphology of the AISI 304 SS. In this research, grinding was conducted under conditions of V_s = 30 m/s, v_w = 15 m/min, and a = 15 μm. On the other hand, the measured grinding temperature indicated in column B of Table 8 (θ = 542 °C) is in a very good agreement with the value given in Ref 26 and is high enough to generate localized thermal damage at the ground surface.

Concerning the compressive residual stresses measured for wire-brushed surfaces, higher amplitudes can be expected by the optimization of the brush specifications and the brushing conditions. However, it is expected that even at these optimized brushing conditions, as the wire brushing is a superficial surface treatment, the depths of the layers affected by this process remained limited compared with the depths that can be reached by the shot-peening treatment.

4.2 Fatigue Life Improvements Resulting From the Brushing Process

The results of the fatigue tests conducted in this investigation comparing the fatigue behavior of the ground and the

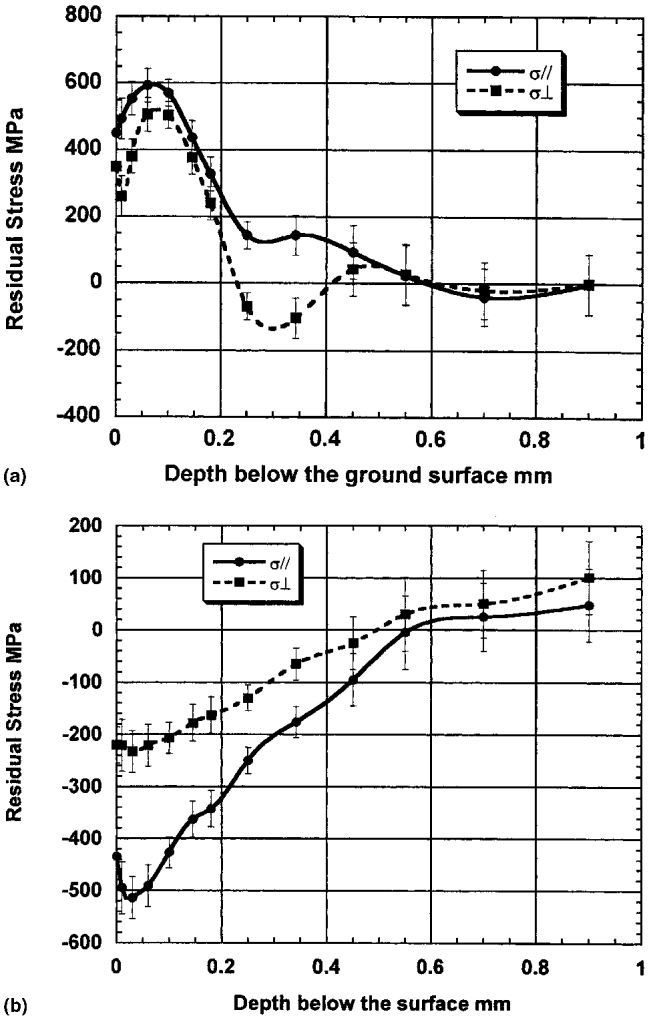

Fig. 7 **(a)** Residual stress profiles for the ground surface of the AISI 304 SS (v_w = 6 m/min; a = 5 μm). **(b)** Residual stress profiles for the wire-brushed surface of the AISI 304 SS (V_s = 800 rpm; V_f = 50 mm/min; N = 10 passes)

wire-brushed surfaces have shown longer lifetimes at 2 × 10^6 cycles for the wire-brushed ones. These fatigue resistance improvements can be explained by the enhancements of the ground surface integrity resulting from the application of the wire-brushing process to these surfaces. Indeed, the fatigue lifetime, and, particularly, the mechanisms of fatigue crack nucleation and first-stage propagation of mechanical components subjected to surface loading are mainly controlled by their surface characteristics.[25,26,30-32]

4.2.1 Roughness Effects. Concerning the effects of the generated surface roughness on the fatigue lifetime of mechanical components, it was reported that the fatigue resistance could be affected significantly by this parameter.[25,26] Indeed, the fatigue resistance could be varied within an order of magnitude when surface roughness was varied using different machining methods, such as forging, grinding, and polishing.[25] In this investigation, it was observed that the high and sharp valleys, which are characteristic of the ground surface topography, constitute potential sites for fatigue crack initiation, as they are considered to be prime locations for microstress concentration.[26] Indeed, the fatigue

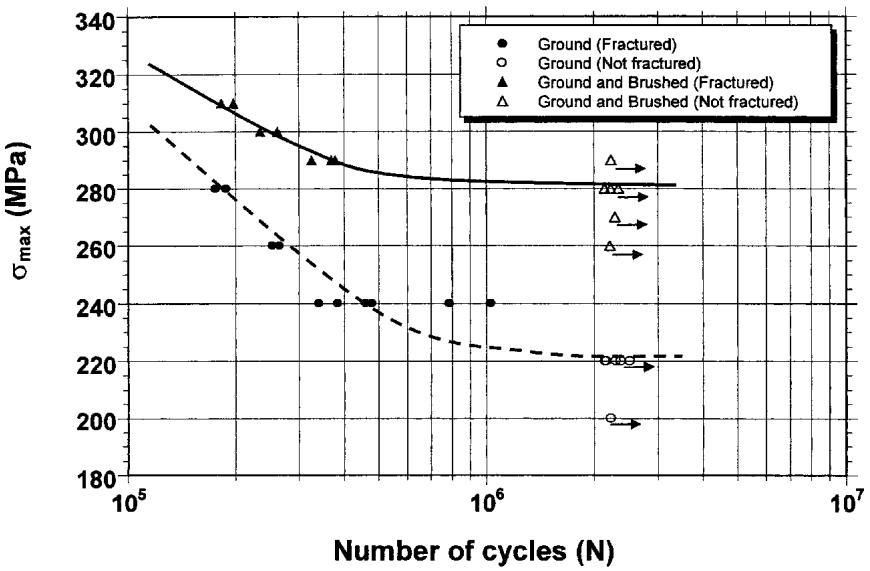

Fig. 8 Fatigue lifetime improvements by wire brushing of the ground surfaces of the AISI 304 SS specimen

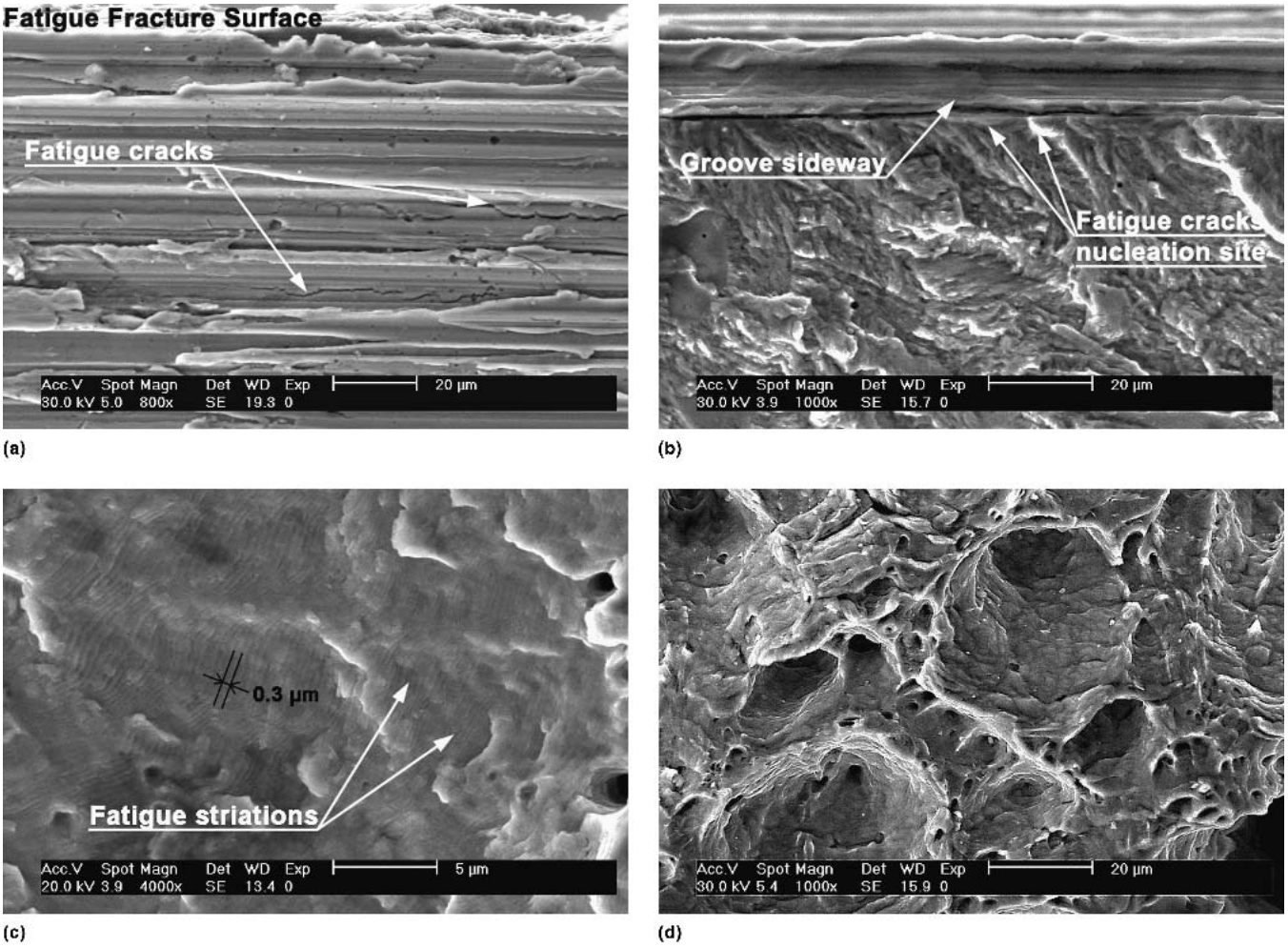

Fig. 9 **(a)** Surface fatigue crack distribution at a distance of 30 μm from the main fracture. **(b)** Fracture facet showing fatigue crack nucleation sites. Arrows indicate that the crack nucleation likely occurred at the bottom of the grinding grooves. **(c)** Fatigue striations at a depth of 800 μm below the ground surface, indicating a crack propagation speed of 0.3 μm per cycle. **(d)** Dimple fracture at a depth of 2 mm below the ground surface

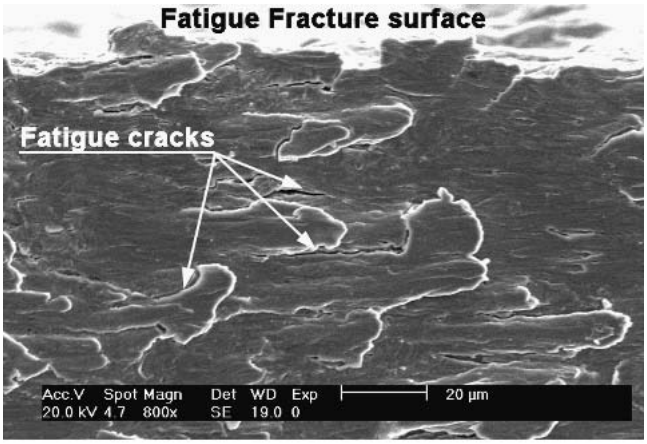

(a)

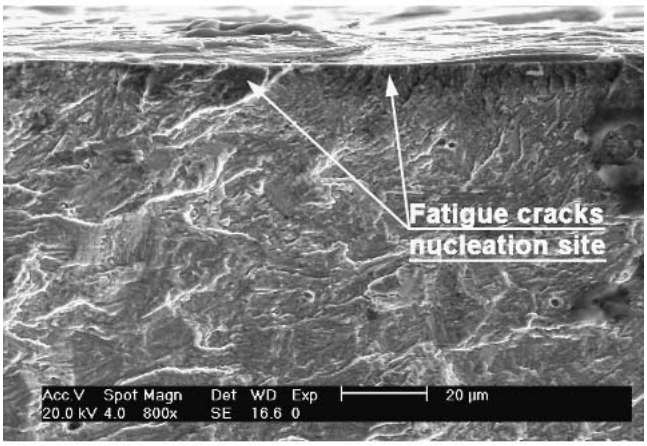

(b)

Fig. 10 **(a)** Fatigue cracks at the brushed surface at a distance of 30 μm from the main fracture of the AISI 304 SS specimen. **(b)** Fracture facet micrograph showing fatigue crack nucleation sites

cracks were seen to initiate at the bottom of these valleys, which correspond to the grinding grooves. Therefore, the generated surface roughness of mechanical components having undergone grinding operation can be considered to be an important parameter that significantly affects their fatigue lifetime.

The application of the wire-brushing process to these surfaces results in a smoother surface topography. It, thus, has a lower level of R_t and is less sensitive to the surface roughness as a factor affecting fatigue crack nucleation.

4.2.2 Work Hardening Effects. The results of investigations related to the effects of near-surface work hardening on fatigue behavior have shown that the amplitude of the hardening, and the corresponding depths of the affected layers, are the main parameters controlling, respectively, fatigue crack initiation and compressive residual stress relaxation under cyclic loading.[30,31] It was determined that a high surface-hardening amplitude delays fatigue crack nucleation and that a large work-hardening layer results in less compressive residual stress relaxation under the cyclic loading. Consequently, this leads to an increased fatigue lifetime for the mechanical components.[30] In this investigation, it was shown that the application of the brushing process to ground surfaces results in higher

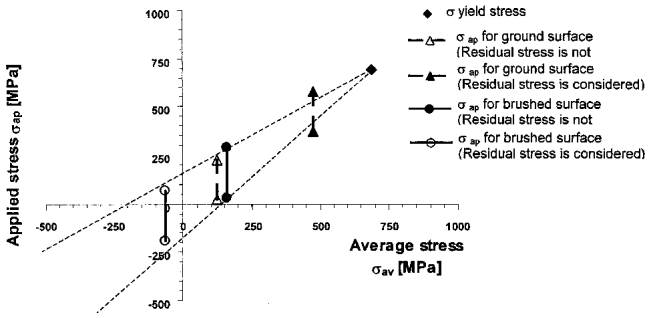

Fig. 11 Diagram of Goodman-Smith showing the effects of the residual stress on the applied cyclic stress σ_{ap} of the ground and brushed surfaces

surface work hardening and a deeper work-hardened layer. Thus, based on the explanations given in Ref 30, the effects of work hardening on the fatigue behavior of wire-brushed AISI 304 SS specimens may be explained as follows: the fatigue strength, which is characterized by the endurance limit σ_D, can be improved by the high amplitude of the surface work-hardened layer, which delays fatigue crack initiation; and the fatigue lifetime, which is characterized by the number of cycles to failure, can be increased by a work-hardened layer that reduces compressive residual stress relaxation under cyclic loading.

4.2.3 Residual Stress Effects. The diagram of Goodman-Smith given in Fig. 11 shows that the presence of residual stresses can affect significantly the fatigue lifetime of mechanical components by altering the effective maximum applied stress ($\sigma_{ap(max)}$) and the minimum applied stress ($\sigma_{ap(min)}$) during fatigue testing. In particular, it is seen that while compressive residual stress, which is generated by the wire-brushing process ($\sigma_\perp = -220$ MPa), lowers the effective applied stresses $\sigma_{ap(max)}$ and $\sigma_{ap(min)}$ ($\sigma_{ap(max)} = 65$ MPa and $\sigma_{ap(min)} = -191.5$ MPa instead of $\sigma_{ap(max)} = 285$ MPa and $\sigma_{ap(min)} = 28.5$ MPa for a theoretical load ratio $R = \sigma_{min}/\sigma_{max} = 0.1$, tensile residual stresses induced by the grinding process ($\sigma_\perp = +350$ MPa) raises $\sigma_{ap(max)}$ and $\sigma_{ap(min)}$ ($\sigma_{ap(max)} = 576$ MPa and $\sigma_{ap(min)} = 372.5$ MPa instead of $\sigma_{ap(max)} = 226$ MPa and $\sigma_{ap(min)} = 22.6$ MPa for a theoretical load ratio $R = 0.1$). This diagram explains the substantial contribution of residual stress regarding improvements in the endurance limit σ_D resulting from the application of the brushing process to ground surfaces.

5. Conclusions

In this investigation, it was shown that mechanical surface treatment by wire brushing of ground AISI 304 SS components could substantially benefit the surface and near-surface integrity of the component. It was seen that this inexpensive and simple process is capable of removing the thermally affected layer induced by grinding and, therefore, eliminates thermal microcracks, microvoids, and sharp grinding grooves. As a result, surfaces with compressive residual stresses, having higher microgeometrical quality and higher hardness, could be generated. When these results were compared with the surface

integrity resulting from the application of the shot-peening process to the AISI 304 SS specimen, it could be concluded that wire-brushed surfaces lead to a higher microgeometrical quality with comparable states of compressive residual stress and surface work hardening. On the other hand, it was seen that the surface integrity enhancements resulting from the application of the wire-brushing process to ground components led to significant improvements in fatigue behavior. Indeed, under the experimental conditions used in this investigation, an improvement of 26% in the endurance limit at 2×10^6 cycles could be realized by the application of the wire-brushing process to the ground components. This value can be increased by further optimization of the wire-brushing parameters, and the corresponding process conditions, particularly for materials with higher mechanical strength characteristics.

References

1. S. Malkin, *Grinding Technology Theory and Application of Machining with Abrasives,* Ellis Horwood Limited, 1989, p 111-112
2. R. Snoeys, M. Maris, and J. Peters, Thermally Induced Damages in Grinding, *Annals of the CIRP,* Vol 27 (No. 2), 1978, p 571-576
3. K.C. Jain, A.N. Kumar, R.N. Mittal, and B.L. Juneja, Surface Integrity of a Hardened and Ground Low-Alloy Steel: Study Based on Surface and Subsurface Damage, *Mater. Sci. Technol.,* Vol 2, 1986, p 856-863
4. D.Y. Jang, T.R. Watkins, K.J. Kozaczek, C.R. Hubbar, and O.B. Cavin, Surface Residual Stress in Machined Austenitic Stainless Steel, *Wear,* Vol 194, 1996, p 168-173
5. S.A. Bentley, A.L. Mantle, and D.K. Aspinwall, The Effect of Machining on the Fatigue Strength of a Gamma Titanium Aluminide Intermetallic Alloy, *Intermetallics,* Vol 7, 1999, p 967-996
6. J.D. Fordham, R. Pilkington, and C.C. Tang, The Effect of Different Profiling Techniques on the Fatigue Performance of Metallic Membranes of AISI 301 and Inconel 718, *Int. J. Fatigue,* Vol 9, 1997, p 487-501
7. G.A. Webster and A.N. Ezeilo, Residual Stress Distribution and Their Influence of Fatigue Lifetimes, *Int. J. Fatigue,* Vol 23, 2001, p S375-S383
8. H. Jia-Wen, Z.H. Zhi, and Z. Ding-quan, Influence of Residual Stress on Fatigue Limit in Various Carbon Steel, *International Conference on Shot Peening ICSP-2,* 14-17 May (Chicago), American Shot Peening Society, 1984, p 340-345
9. K.V. Kumar, R.R. Matarrese, and E. Ratterman, Control of Residual Stress in Production Grinding With CBN, SEA Technical Paper Series No. 890979, *40th Annual Earthmoving Industry Conference,* April 11-13, 1989 (Peoria, IL)
10. N. Ben Fredj, Y. Ichida, K. Kishi, and X. Lei, Wear Mechanism of CBN Wheels in Creep Feed Grinding, *Proceedings of the First China-Japan International Conference on Progress of Cutting and Grinding,* 23-25 Nov (Beijing), International Academic Publisher, 1992, p 227-232
11. E.R. de lois, A. Walley, M.T. Milan, and G. Hammersley, Fatigue Crack Initiation and Propagation on Shot-Peened Surfaces in A316 Stainless Steel, *Int. J. Fatigue,* Vol 17, 1995, p 493-499
12. M. Widmark and A. Melander, Effect of Material, Heat Treatment, Grinding and Shot Peening on Contact Fatigue Life of Carburised Steels, *Int. J. Fatigue,* Vol 21, 1999, p 309-327
13. Y. Ochi, K. Masaki, T. Matsumura, and T. Sekino, Effect of Shot-Peening Treatment on High Cycle Fatigue Property of Ductile Cast Iron, *Int. J. Fatigue,* Vol 23, 2001, p 441-448
14. M.S.A. Torres and H.J.C. Voorwad, An Evaluation of Shot Peening, Residual Stress and Stress Relaxation on the Fatigue Life of AISI 4340 Steel, *Int. J. Fatigue,* Vol 24, 2002, p 877-886
15. M.P. Nascimento, R.C. Souza, W.L. Pigatin, and H.J.C. Voorwald, Effects of Surface Treatments on the Fatigue Strength of AISI 4340 Aeronautical Steel, *Int. J. Fatigue,* Vol 23, 2001, p 607-618
16. I. Altenberger, B. Scholtes, U. Martin, and H. Oettel, Cyclic Deformation and Near Surface Microstructures of Shot Peened or Deep Rolled Austenitic Stainless Steel AISI 304, *Mater. Sci. Eng.,* Vol A264, 1999, p 1-16
17. P. Peyer, R. Fabbro, P. Merrien, and H.P. Lieudare, Laser Shot Processing of Aluminum Alloys. Application to High Cycle Fatigue Behavior, *Mater. Sci. Eng.,* Vol A210, 1996, p 102-113
18. L.W. Tsay, M.C. Young, M. C. Young, and C. Chen, Fatigue Crack Growth Behavior of Laser-Processed 304 Stainless Steel in Air and Gaseous Hydrogen, *Corrosion Sci.,* Vol 45 (No. 9), 2003, p 1985-1997
19. P.S. Prevéy and J.T. Cammett, Low Cost Corrosion Damage Mitigation and Improved Fatigue Performance of Low Plasticity Burnished 7075-T6, *J. Mater. Eng. Perf.,* Vol 10, 2001, p 548-555
20. Y.F. Kudryavtsev, P.P. Mikheev, and V.F. Korshun, Influence of Plastic Deformation and Residual Stresses, Created by Ultrasonic Impact Treatment, on the Fatigue Strength of Welded Joints, *Paton Weld. J.,* Vol 12, 1995, p 3-7
21. G. Jaeger, I. Endler, K. Bartsch, M. Heilmaier, and A. Leonhardt, Fatigue Behavior of Duplex Treated $TiC_x\ N_{1-x}$ - and $Ti_{1-x}\ A_x$ N-hard Coating Steel Compounds, *Surf. Coat. Technol.,* Vol 150, 2002, p 282-289
22. K. Genel, M. Demirkol, and M. Capa, Effect of Ion Nitriding on Fatigue Behaviour of AISI 4140 Steel, *Mater. Sci. Eng. A,* Vol 279, 2000, p 207-216
23. R.J. Stango, S.M. Heinrich, and C.Y. Shia, Analysis of Constrained Filament Deformation and Stiffness Properties of Brushes, *ASME J. Eng. Indust.,* Vol 111, 1989, p 238-243
24. A. Ben Rhouma, C. Braham, M.E. Fitzpatrick, J. Lédion, and H. Sidhom, Effects of Surface Preparation on Pitting Resistance, Residual Stress, and Stress Corrosion Cracking in Austenitic Stainless Steel, *J. Mater. Eng. Perf.,* Vol 10 (No. 5), 2001, p 507-514
25. S. Andrews and H. Sehigolo, A Computer Model for Fatigue Cracks Growth From Rough Surfaces, *Int. J. Fatigue,* Vol 22, 2000, p 619-630
26. P.S. Maiya and D.E. Bush, Effect of the Surface Roughness on Low-Cycle Fatigue Behavior of Type 304 Stainless Steel, *Metall. Trans. A,* Vol 6, 1975, p 1761-1774
27. M. Obata and A. Sudo, Effect of Shot Peening on Residual Stress and Corrosion Cracking for Cold Worked Austenitic Stainless Steel, *International Conference on Shot Peening ICP-5,* D. Kirk, ed., Sept 13-17, 1993 (Oxford, UK), p 257-264
28. L. Jiang, J. Paro, and H. Hannu, Comparison of Grindability of HIPped Austenitic 316L, Duplex 2205 and Super Duplex 2507 and As-Cast 304 Stainless Steels Using Alumina Wheels, *J. Mater. Proc. Technol.,* Vol 62, 1996, p 1-9
29. S. Yossifon and C. Rubenstein, The Grinding of Workpieces Exhibiting High Adhesion: Part 1. Mechanism, *ASME J. Eng. Indust.,* Vol 103, 1981, p 145-155
30. W.Z. Zhuang and G.R. Halford, Investigation of Residual Stress Relaxation Under Cyclic Load, *Int. J. Fatigue,* Vol 23, 2001, p S31-S37
31. L. Lawson, E.Y. Chen, and M. Meshii, Near-Threshold Fatigue: A Review, *Int. J. Fatigue,* Vol 21, 1999, p S15-S34
32. I. Altenberger, B. Sckotes, U. Martin, and H. Oettel, Cyclic Deformation and Near Surface Micostructures of Shot Peened or Rolled Austenitic Stainless Steel AISI 304, *Mater. Sci. Eng.,* Vol A264, 1999, p 1-16